J Mater Sci (2009) 44:6110–6116
DOI 10.1007/s10853-009-3845-5

Nitrogen-substituted TiO_2: investigation on the photocatalytic activity in the visible light range

Franck Tessier · Cordt Zollfrank · Nahum Travitzky · Hans Windsheimer · Odile Merdrignac-Conanec · Jean Rocherullé · Peter Greil

Received: 10 July 2009 / Accepted: 25 August 2009 / Published online: 10 September 2009

Abstract Nitrogen-doped titanium oxides are attractive materials for the degradation of organic pollutants in water due to their photocatalytic activity in the visible light range. The evolution of the photocatalytic properties was studied on a number of TiO_xN_y powder samples where x varied from 2 to 0 (TiO_2 to TiN) through increasing the nitrogen content ($y = 0$–1). X-ray diffraction and Raman spectroscopy showed that an anatase type TiO_xN_y was obtained at low nitrogen contents (<2 wt%). With increasing nitrogen content a structural transition from anatase to cubic TiN was observed. Electron spin resonance measurements of the TiO_xN_y samples confirmed the presence of unpaired electrons and defects for the TiO_xN_y materials with low nitrogen content (<2 wt%). The photo-induced activity of the TiO_xN_y materials was evaluated under VIS illumination of solutions containing methylene blue as an organic probe. The TiO_xN_y samples exhibited an improved photocatalytic activity under visible light illumination compared to TiO_2 at nitrogen levels lower than 2 wt%. A photocatalytic activity could not be detected at nitrogen levels higher than 10 wt% and after conversion of the TiO_xN_y into the cubic phase. Optimum photocatalytic activity in the visible range can be achieved at nitrogen levels lower than 2 wt% for TiO_xN_y materials.

F. Tessier (✉) · O. Merdrignac-Conanec · J. Rocherullé
UMR CNRS 6226 "Sciences Chimiques de Rennes", équipe "Verres et Céramiques", groupe "Matériaux Nitrures", Université de Rennes 1, 35042 Rennes Cedex, France
e-mail: Franck.Tessier@univ-rennes1.fr
URL: www.verceram.univ-rennes1.fr

C. Zollfrank · N. Travitzky · H. Windsheimer · P. Greil
Department of Materials Science and Engineering-3, Glass and Ceramics, Friedrich-Alexander University of Erlangen-Nürnberg, Martensstr 5, 91058 Erlangen, Germany
URL: http://www.glass-ceramics.uni-erlangen.de/

Introduction

Titanium dioxide (TiO_2) in the anatase crystallographic modification is a well-known efficient photocatalyst in numerous applications such as antibacterial agent, as self-cleaning surfaces or in water and air purification [1]. UV light irradiation of TiO_2 with photon energies higher than the bandgap ($\sim$3 eV) gives rise to the generation of electron–hole pairs. If the charge carriers do not recombine, they can migrate to the surface where titanium atoms and holes at superficial OH groups trap electrons. Trapped holes form OH radicals and trapped electrons react with O_2 and H_2O to form HO_2 radicals. These free radicals are very oxidant entities and can cause the degradation of organic compounds into CO_2 and H_2O [2]. For irradiation with wavelengths in the near UV range up to 390 nm, TiO_2 exhibits an improved chemical stability and a high photocatalytic activity. The UV-photocatalytic activity of several oxides such as the wide-gap semiconductors $SrTiO_3$ (3.4 eV) or $NaTaO_3$ (4.0 eV) has been widely reported in literature [3, 4]. UV light irradiation results in generation of electron–hole pairs by photoexcitation. Since solar light UV availability is less than 5%, numerous studies have been performed over the last years to extend the sensibility of photocatalytic materials towards visible light. Semiconductors with a smaller bandgap, e.g. WO_3 and CdS, absorb visible radiation, but their performance as photocatalysts for applications in water splitting is limited due to their instability versus photocorrosion [5]. The water photolysis and the production of hydrogen H_2 are also interesting applications of solar energy [6–8].

Nitrides and oxynitrides are attractive materials with their electronic structure and optical properties directly related to the nitrogen substitution [9]. The nitrogen (N^{3-}) to oxygen (O^{2-}) substitution involves an increase in the

covalent character resulting in specific colour changes [10, 11]. While a number of oxides are white-coloured powders (absorption in the UV), many nitrides show a pronounced absorption in the visible range. Since colour is determined by the position of the absorption edge a shift towards higher wavelengths can result in absorption in the visible part of the spectrum. The colour of nitride-type compounds is explained by a decrease in the band gap energy value, as confirmed by band structure calculations. We can already take into account the difference in the energy level of the oxygen and nitrogen 2p orbitals: $E_{2p}(O) = -14.8$ eV, $E_{2p}(N) = -13.4$ eV (top of the valence band) to simply explain this decrease between valence and conduction bands. However, concerning slightly doped oxides with nitrogen, a controversy exists about the mechanism explaining the observed red shift of the position of the absorption edge. Some studies argue for a narrowing of the band gap of the TiO_2 precursor, while others support the formation of coloured centers and the corresponding presence of localized states of the dopant within the bandgap [12, 13]. Oxynitrides are promising materials for visible-light-driven photocatalysis [11, 14–17]. Another photocatalytic reaction of interest concerns the degradation of organic molecules on nitrogen-doped titanium oxide in water and air [14]. Though doping of TiO_2 with nitrogen incorporation by different methods allows shifting the absorption edge of TiO_2 towards smaller energies, the activity of the photocatalyst under visible light, however, strongly depends on the preparation route [17–20]. Most of the published data were focused on N-doped TiO_2 with low nitrogen contents (<2 wt%). Since nitrogen has a vital effect on the photocatalytic activity in the visible light range, the objective of the present work is to explore the degradation of organic compounds as a function of the nitrogen content in TiO_2. In addition, the influence of the specific surface area (A_{sp}) on the photocatalytic activity and the effect of the pH-value on the degradation were investigated. Both parameters are crucial for catalysed photoinduced reactions: A_{sp} is directly related to the number of available catalytically active sites and the pH-value has a strong impact on the surface potential of the catalyst particles which is important for the interaction between dissolved compounds and catalyst particles [21, 22]. To assess the photocatalytic characteristics of titanium oxynitrides TiO_xN_y, we prepared a number of powder samples with systematically varied nitrogen content. The phase composition was evaluated by X-ray diffractometry and element analysis. The samples were characterised by Raman microspectroscopy and electron spin resonance (ESR). The photostimulated degradation of methylene blue (MB) under visible (Vis) light illumination was determined by Vis-spectroscopy versus time of exposure. The degradation was measured at pH values of 7 and 9 and will be discussed with respect to the measured zeta potential ζ. The obtained data were correlated with the A_{sp} evaluated from BET measurements.

Experimental

Thermal nitridation

A number of titanium oxynitrides were prepared from anatase TiO_2 (pure quality, Labosi, OSI, F). Nitridation reactions were carried out in alumina boats placed inside an electrically heated furnace through which ammonia gas flowed with a flow rate of 20 L h^{-1}. The temperature was raised up to 1000 °C at a heating rate of 10 °C min^{-1}. After 6 h reaction time, the furnace was switched off and the nitrided powders were cooled to room temperature under pure nitrogen atmosphere.

X-ray diffraction

XRD powder patterns were recorded between 10 and 80° using a Philips PW3710 diffractometer (Almelo, NL) operated with Cu K_α radiation ($\lambda = 1.5418$ Å) with a scan rate of 2.4°/min. X'PERT softwares (Philips, Almelo, NL)—Data Collector, and Graphics and Identify—were used for pattern recording, analysis and phase matching, respectively. The lattice parameters were refined using the *Dicvol* software (Rennes, F) [23].

Element analysis

Oxygen and nitrogen contents (x, y in TiO_xN_y) were determined with a LECO® TC-600 analyser (St Joseph, USA) using the inert gas fusion method. Nitrogen was measured as N_2 by thermal conductivity and oxygen as CO_2 by infrared detection. The apparatus was calibrated using standard oxides (SiO_2 and ZrO_2), Si_2N_2O and ε-TaN as nitrogen standard [24].

Raman spectroscopy

TiO_xN_y powder samples were analysed by confocal Raman microscopy (Almega XR, Thermo Fisher, Dreieich, D) using an excitation laser with a wavelength of 780 nm. The spectra were collected from a region of interest of the powder particles between 150 and 1000 cm^{-1} at a resolution of 2 cm^{-1}.

Electron spin resonance

Electron spin resonance spectra (Bruker ESP 300A, Karlsruhe, D) measurement of the TiO_2 and the TiO_xN_y

powder samples were obtained at room temperature in air in the X-band (9.7 Ghz). The applied microwave power was 63.6 mW and the modulation frequency was 100 kHz.

BET measurement

N_2 sorption isotherms were measured using a surface area analyser (ASAP 2000, Micromeritics, Mönchengladbach, D). The pore size distribution was calculated from the adsorption branch by the BJH (Barett-Joyner-Halenda) method. Specific surface areas A_{sp} were calculated by the BET (Brunauer-Emmett-Teller) method.

Zeta potential ζ

The zeta potential ζ of the powder suspensions (2 wt%) was measured with an electrokinetic sonic analysis system (Field ESA, PA Partikel-Analytik-Meßgeräte, Frechen, D). The titration was performed with 1M HCl and 1M NaOH solutions. The particle size of the respective powders required for evaluation of the zeta potential ζ was determined using a Mastersizer 2000 (Malvern Instruments, Herrenberg, D).

Photocatalytic degradation

Approximately 1.25 mg of methylene blue (MB) was dissolved in 100 mL of distilled water (Chromasolv G, Sigma–Aldrich, Steinheim, D) with a pH of 7 in a standard borosilicate glass beaker (cut off wavelength 300 nm). For some experiments, the pH of the sample solution was buffered to a pH value of 9. After adding the respective amount of the catalyst powder (50 mg) the magnetically stirred suspension was illuminated with a conventional halogen quartz lamp (12 V, 50 W, 38°). The lamp was placed at a distance of 9 cm to an iris shutter with an opening of 2 cm, which was located at a distance of 1 cm from the beaker containing the reaction solution. This experimental setup avoided undesired heating of the sample solution. A quantity of 20 mL of the MB solution was extracted directly after mixing the components (0 min) and after 40, 80 and 120 min. The sample suspension was centrifuged and the corresponding absorption spectra of the clear MB solution were measured in a UV–Vis spectrometer (Lamda 19, Perkin Elmer, Waltham, D) between 450 and 800 nm. The value of the adsorption maximum located between 660 and 670 nm was used to determine the MB concentration. After the absorption measurement, the centrifuged catalyst was re-suspended and the MB sample suspension was returned to the visible illuminated bulk suspension. TiO_2 (P25, Degussa, Essen, D) was used as a reference catalyst powder.

Results and discussion

Preparation of the TiO_xN_y powders

A series of oxynitride samples TiO_xN_y were prepared with compositions ranging from anatase TiO_2 to cubic face centred TiN by progressively substituting nitrogen for oxygen, Table 1. Element analyses indicate low nitrogen content within the anatase structure at temperatures lower than 650 °C. The corresponding colour of the samples turns from white to pale yellow as soon as nitrogen is introduced, however, darkens rapidly with increasing nitrogen content. A change in the colour of the powders at a reaction temperature of 650 °C was observed. Exceeding this specific temperature coincides also with the presence of a mixture of oxynitride anatase-type and TiN-type phase, Fig. 1. Both structures coexist in the temperature range from 600 to 750 °C. The darkening of the colour from white (TiO_2) to black and golden brown (TiN) is primarily due to a well-known phenomenon attributed to

Table 1 Nitridation reaction experimental parameters of TiO_2 anatase samples with temperature

Sample code	Reaction temperature (°C)	Crystal structure	O (wt %)	N (wt %)	Chemical formula
A	500	Anatase	38.9	0.11	$TiO_{1.91}N_{0.01}$
B	520	Anatase	36.46	0.41	$TiO_{1.73}N_{0.02}$
C	570	Anatase	35.75	0.53	$TiO_{1.68}N_{0.03}$
D	650	Anatase + cubic	34.4	2.17	$TiO_{1.62}N_{0.12}$
E	670	Anatase + cubic	33.4	3.73	$TiO_{1.59}N_{0.20}$
F	700	Anatase + cubic	28.3	8.2	$TiO_{1.33}N_{0.44}$
F-1	750	Cubic	13.1	18.3	$TiO_{0.57}N_{0.91}$
F-2	800	Cubic	10.9	18.5	$TiO_{0.46}N_{0.90}$
G	870	Cubic	7.57	19.87	$TiO_{0.31}N_{0.95}$
H	1050	Cubic	1.3	21.9	$TiO_{0.05}N_{0.97}$
I	Commercial sample	Cubic	0.92	22.05	$TiO_{0.04}N_{0.98}$

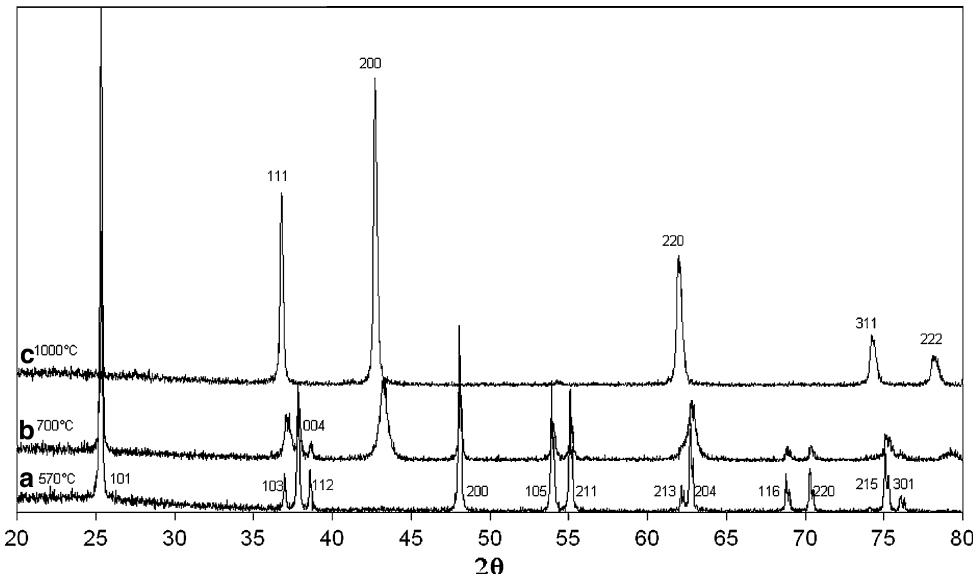

Fig. 1 XRD patterns of nitrided samples from 500 to 1000 °C. (**a**) N-doped anatase TiO_2 (0.5 wt% N), (**b**) mixture between anatase N-doped TiO_2 and cubic TiO_xN_y (3.7 wt% N), (**c**) cubic TiO_xN_y (21.9 wt% N)

the presence of mixed valence states of titanium, Ti(IV) and Ti(III).

Raman spectroscopy

The Raman spectroscopic characteristics of TiO_xN_y powders were investigated to monitor the phase development as a function of the nitrogen content, Fig. 2. Anatase exhibits six Raman active modes: one A_{1g}, two B_{1g} and three E_g. At low nitrogen contents (0.1–0.5 wt% N) these typical Raman bands for anatase type titania materials were observed at 144 cm^{-1} (E_g), 198 cm^{-1} (E_g), 397 cm^{-1} (B_{1g}), 516 cm^{-1} (two bands: $A_{1g} + B_{1g}$) and 639 cm^{-1} (E_g) [25]. With increasing nitrogen content up to 4.1 wt% N corresponding to a mixture of anatase and TiN cubic types a blue shift occurred for three bands by approximately 9–389 cm^{-1}, 507–628 cm^{-1}. However, the other two bands at lower energies (144, 198 cm^{-1}) did not show a change of position. New strong and broad bands located at 241 and 438 cm^{-1} were developed at a nitrogen concentration of 19.9 wt% N where the corresponding powder presents only the cubic TiN type. The very strong band at 144 cm^{-1} remained unchanged, while the bands at 389 and 507 cm^{-1} were only visible as shoulders on the two newly developed bands. The band at 507 cm^{-1} was broadened and the band at 628 cm^{-1} experienced a blue shift by 17–609 cm^{-1}. At a phase composition with 20.5 wt% N new broad peaks occurred in the Raman spectra at 206 and 553 cm^{-1}, which were assigned to the transverse acoustic (TA), and transverse optical (TO) modes of the cubic TiN [26]. A broad band was observed as a shoulder between 290 and 340 cm^{-1} corresponding to the longitudinal acoustic (LA) mode. These results corroborate the Raman data given for stoichiometric and non-stoichiometric TiN_y where y was varied from 0.55 to 0.95 [27]. The spectrum obtained for $TiN_{0.8}$ particularly shows a good similarity with the data we present. In our work three different characteristic Raman spectra were identified depending on the composition of the TiO_xN_y powders. If the TiO_xN_y powder exhibits an anatase structure, the typical appearance of the corresponding Raman shifts for TiO_2 was observed. A different spectroscopic pattern was observed when both phases—anatase and the cubic TiN—coexist according to the XRD analysis. The expected Raman shifts for cubic TiN were observed at contents of nitrogen higher than 21.0 wt%.

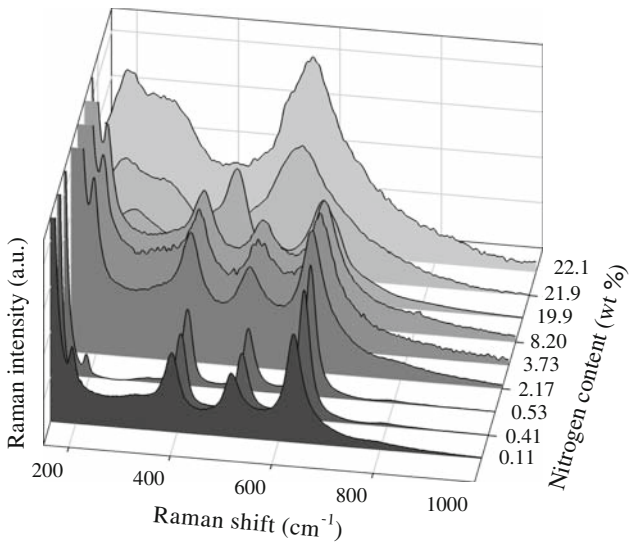

Fig. 2 Raman spectra of TiO_xN_y powders with increasing nitrogen content from 0.11 to 22.1 wt% N

Electron spin resonance (ESR)

ESR measurements were performed on the TiO_xN_y powders as a function of the nitrogen content to investigate the possible existence of localized defects responsible for the photocatalytic activity. The first derivative (D1) ESR spectra of selected TiO_xN_y samples are shown in Fig. 3. The ESR spectrum of TiO_2 exhibits a resonance at 346 mT ($g = 2.001$; free electron $g = 2.0023$) and at 354 mT ($g = 1.956$). The positions of the peaks in the first derivative curve and the line shape of the ESR signal from pure TiO_2 are similar to the results published in literature, where the ESR signal at 346 mT was assigned to surface adsorbed O_2^- species [28, 29]. The ESR spectrum of 0.4 wt% N shows the same line shape as it was described for TiO_2. This indicates that nitrogen doping has only a little effect on the defect structure of TiO_xN_y material. However, a shift of the ESR resonance from 346 to 343 mT ($g = 2.018$) is observed for a nitrogen concentration of 1.3 wt% while the resonance at 354 mT had vanished, although the observed crystal structure according to XRD was still found to be anatase. Interestingly, the line shape of measured spectrum at this composition shows an analogous behaviour as it is described for irradiated ($\lambda > 420$ nm) nitrogen doped TiO_2 [29]. The observed resonance has been identified as a trapped hole at an oxygen centre (oxygen hole centre OHC), which is covalently bound to titanium atoms near the surface [30]. This signal is much stronger in N-modified TiO_2 due to the cleavage of Ti–O–Ti bonds during nitridation and generation of the OHC due to unsaturated valences [28]. However, the intensity of resonance at 343 mT decreases with increasing nitrogen content up to 8.1 wt%. Simultaneously, the structural transition from anatase to cubic TiN type occurs. This indicates that the transition from anatase to cubic TiN results in a loss of surface confined defects related to vacancies or radicals. ESR signals could not be detected for TiO_xN_y samples with a nitrogen content higher than 15 wt%. TiN materials also did not show any ESR signal. If a defect structure such as radicals or hole centres are considered to be required for the photodegradation of organic compounds, it can be concluded, that photocatalytic activity will be limited to TiO_xN_y materials with a nitrogen content lower than ~1.5 wt%.

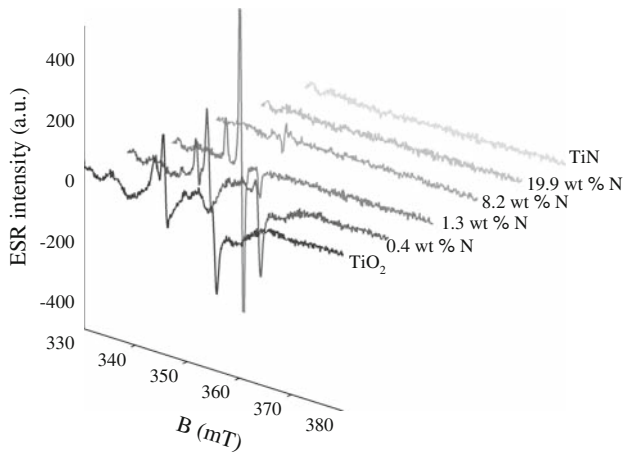

Fig. 3 First derivative ESR spectra of TiO_2, TiO_xN_y with varied nitrogen content and TiN powders

Photocatalytic activity of TiO_xN_y

Experiments under UV illumination indicated that TiO_2 doped with low contents of nitrogen up to 0.4 wt% N showed a substantial decrease of the photocatalytic activity with respect to the reference material TiO_2 (P25). These results were unexpected since at these doping levels the TiO_xN_y powders still maintained the anatase structure. Other authors also found that the UV-light activity of nitrogen-doped titania catalysts ($TiO_{1.96–1.90}N_{0.04–0.10}$) with a yellowish colour was to be less effective than that of pure titania [31]. However, the photocatalytic properties apparently strongly depend on the nitrogen content of the TiO_xN_y. Nitrogen doping of titania should lead to a modest bandgap narrowing by an anodic shift of the conduction band edge and to the generation of a number of surface states that are located close to the valence band edge, which should result in photocatalytic activity under visible light illumination [14, 17, 32]. Therefore, all experiments were conducted under visible light illumination, which is more related to polluted water purification situation. The MB degradation experiments with TiO_2 and TiO_xN_y catalyst powder were carried out under VIS illumination at pH = 7 in water and in two cases in buffered solution at pH = 9. The degradation rate r [$(dc_{MB})/dt$] was determined from the decrease of the MB concentration with time by regression analysis. Furthermore, it is assumed that a high specific area A_{sp} exhibits a large fraction of catalytically active sites, which should result in an increased degradation rate r. In order to compare different photoactive catalyst powders of varying particles sizes, the experimental degradation rates r are correlated to the specific surface area A_{sp} of the respective sample, Table 2. The A_{sp} corrected degradation rates r_{corr} for the TiO_xN_y materials with a nitrogen content of up to 2 wt% are higher than that for the TiO_2 reference. This can be explained by the decrease of the band gap energy value, which shifts the generation of electron–hole pairs to lower photon energies into the visible light range. At higher nitrogen levels than 2 wt%, the degradation of MB is lower than for the TiO_2 reference. This observation coincides with the beginning phase transformation from the anatase into the cubic structure as confirmed by XRD and Raman spectroscopy, Figs. 1 and 2.

Table 2 Experimental and calculated data for the degradation of MB under visible light illumination for TiO_2 and the TiO_xN_y powder samples

	Time (min)	pH = 9 TiO_2	pH = 7 TiO_2	pH = 9 0.4 (wt% N)	pH = 7 0.4 (wt% N)	pH = 7 0.5 (wt% N)	pH = 7 1.3 (wt% N)	pH = 7 2.2 (wt% N)	pH = 7 4.1 (wt% N)
Absolute concentration c_{MB} (g/L) × 10^{-3}	**0**	12.5	12.9	12.5	12.6	13.2	12.1	11.7	9.6
	40	8.9	11.2	10.8	11.2	11.9	12.5	11.7	10.1
	80	6.1	9.3	9.1	9.3	11.2	11.7	10.9	9.5
	120	3.2	8.1	7.4	7.8	10.4	11.0	10.3	9.0
Degradation rate r (g/L × min) × 10^{-6}		7.7	4.1	4.2	4.0	2.3	1.0	1.3	0.6
A_{SP} (m^2/g)		50.4	50.4	11.0	11.0	11.00	12.00	13.00	13.00
m_{cat} (g)		0.05	0.05	0.05	0.04	0.03	0.05	0.05	0.05
A_{SP} and m_{cat} corrected degradation rate r_{corr} (g/L × min) × 10^{-6}		3.1	1.6	7.7	7.3	5.8	2.8	2.0	0.9

Additionally, ESR analysis also showed a change in the defect structure of the TiO_xN_y material at these nitrogen contents. The defect structure similar to TiO_2 was found at low nitrogen contents (0.5 wt%) by ESR analysis. Obviously, the generation of electron–hole pairs is comparable for these materials, since the defect structure can be related to surface located O_2^--species and OHC [28–30]. At higher nitrogen contents the ESR spectra changed and the electronic defects related to unpaired electrons finally vanished at nitrogen levels higher than 8 wt% N. At the same time the Raman spectra showed a second transformation of phases from the anatase/cubic mixture into single phase cubic which was also confirmed by XRD observation. A distinct photocatalytic activity could not be observed for high nitrogen contents and TiN-based materials.

It was shown that the degradation of MB was influenced by the pH and accelerated at a basic value of nine, Fig. 4. The MB molecules are positively charged due to the amino functions so that adsorption should be facilitated when the catalyst particles are negatively charged. Figure 5 shows the effect of the pH on the zeta potential ζ for TiO_2 and TiO_xN_y with a nitrogen content of 0.5 wt%. Compared to the zeta potential values ζ for TiO_2 of −44 mV (pH = 7) and −103 mV (pH = 9), TiO_xN_y with a nitrogen content of 0.5 wt% showed considerably lower zeta potentials ζ with −9 mV at pH 7 and −37 mV at pH 9. It can be deduced that with an increased negative potential the activity of the catalysts is likewise increased due to improved adsorption of MB on the particles.

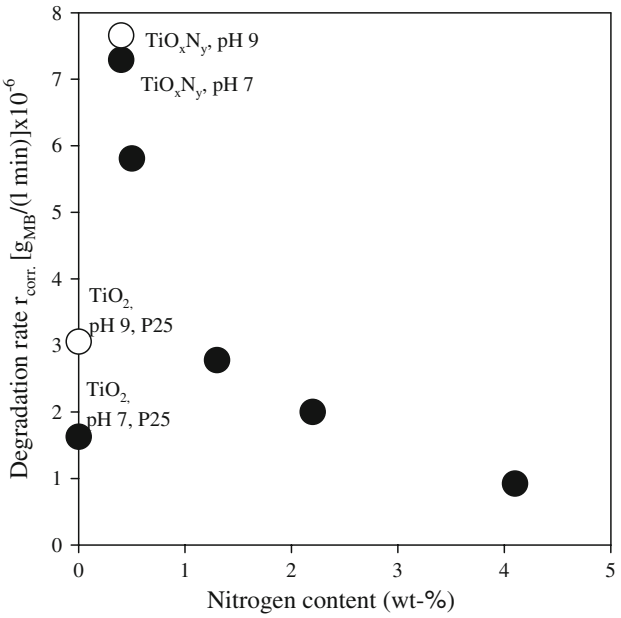

Fig. 4 Photocatalytic degradation of MB under visible light illumination of TiO_xN_y powders and TiO_2 (P25) at pH 7 and 9 corrected for the specific surface area, the values are related to an amount of 1×10^{-3} g applied catalyst powder

Conclusions

Various TiO_xN_y powders with phase composition systematically varied from $x = 0$–2 to $y = 0$–1 were prepared to investigate the photocatalytic degradation of organic compounds. The TiO_xN_y catalyst powders showed an improved photocatalytic activity compared to TiO_2 under visible illumination at nitrogen levels lower than 2 wt%. This effect is due to a smaller band gap, which allows the generation of electron–hole pairs necessary for photodegradation at lower photon energies. At higher nitrogen contents, the photocatalytic activity drastically decreased and vanished at 8 wt% N. Our study distinctly showed that the photocatalytic activity is directly connected to the anatase modification of the TiO_xN_y materials. The degradation rates strongly decrease when a mixture of anatase and a cubic polymorph coexist at 2 wt% N as confirmed by

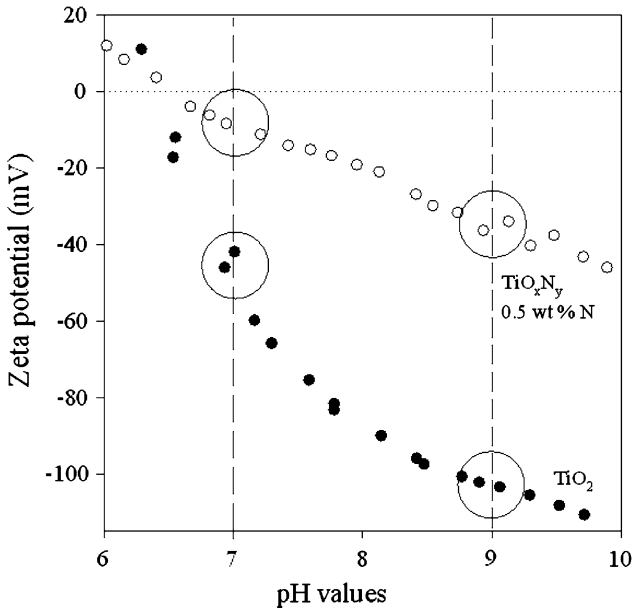

Fig. 5 Zeta potential ζ of a representative TiO_xN_y powder (0.5 wt% N) and TiO_2 (P25) at pH 7 and 9

XRD and Raman studies. At the same time the defect structure accompanied with a low field shift of the ESR resonance of the TiO_xN_y material changed with a nitrogen content of 2 wt% N in the range were both structural phases anatase and cubic TiN coexist. The subsequent decrease of the ESR signals due the structural transition is accompanied by a reduction of the photocatalytic activity as a consequence of increasing nitrogen content. The photodegradation characteristics completely vanished after conversion of the TiO_xN_y into the cubic phase at 10 wt% N. Additionally, paramagnetic defects could not be detected. It can be concluded from the obtained data that vacancy defects were already present in the synthesised TiO_xN_y at low nitrogen doping levels up to 0.5 wt% even without irradiation. These materials appear to be superior photocatalysts under visible light illumination compared to the TiO_2.

Acknowledgements Financial support from the bilateral program Procope (2006–2007) between Egide-French Foreign Affairs and the German Academic Exchange Service (DAAD) is gratefully acknowledged.

References

1. Kaneko M, Okura I (2002) Photocatalysis: science and technology. Springer, Kodansha, p 109
2. Boujday S, Wünsch F, Portes P, Bocquet JF, Colbeau-Justin C (2004) Sol Energy Mater Sol Cells 83:421
3. Kudo A, Kato H, Tsuji I (2004) Chem Lett 3:1534
4. Domen K, Hara M, Kondo JN, Takata T, Kudo A, Kobayashi H, Inoue Y (2001) Korean J Chem Eng 18:862
5. Hitoki G, Takata T, Kondo JN, Hara M, Kobayashi H, Domen K (2002) Electrochemistry 70:463
6. Bahnemann D (2004) Sol Energy 77:445
7. Licht S (2003) J Phys Chem B 107:4253
8. Kudo A (2007) Int J Hydrogen Energy 32:2673
9. Marchand R, Tessier F, Le Sauze A, Diot N (2001) Int J Inorg Mater 3:1143
10. Tessier F, Marchand R (2003) J Solid State Chem 171:143
11. Tessier F, Maillard P, Cheviré F, Domen K, Kikkawa S (2009) J Ceram Soc Jap 117(1):1
12. Serpone N (2006) J Phys Chem B 100:24287
13. Irie H, Watanabe Y, Hashimoto K (2003) J Phys Chem B 107:5483
14. Asahi R, Morikawa T, Ohwaki T, Aoki K, Taga Y (2001) Science 293:269
15. Maeda K, Domen K (2007) J Phys Chem C 111:7851
16. Li D, Haneda H (2004) J Photochem Photobiol A Chem 160:203
17. Li D, Haneda H, Hishita S, Ohashi N (2005) Mater Sci Eng B 117:67
18. Beranek R, Kisch H (2008) Photochem Photobiol Sci 7:40
19. Nishijima K, Ohtani B, Yan X, Kamai T, Chiyoya T, Tsubota T, Murakami N, Ohno T (2007) Chem Phys 339:64
20. Martinez-Ferrero E, Sakatani Y, Boissière C, Grosso D, Fuertes A, Fraxedas J, Sanchez C (2007) Adv Funct Mater 17:3348
21. Andreozzi R, Caprio V, Insola A, Marotta R (1999) Catal Today 53:51
22. Bhattacharjee S, Shah YT (1998) Rev Chem Eng 14:1
23. Boultif A, Louer D (1991) J Appl Cryst 24:987
24. Gruner W, Wollein B, Lengauer W (2004) Microchim Acta 146:1
25. Tompsett GA, Bowmaker GA, Cooney RP, Metson JB, Rodgers KA, Seakins JM (1995) J Raman Spectrosc 26:57
26. Ding ZH, Yao B, Qiu LX, Lv TQ (2006) J Alloys Compd 421(1–2):247
27. Spengler W, Kaiser R, Christensen AN, Mueller-Vogt G (1978) Phys Rev B Solid State 17(3):1095
28. Prokes SM, Gole JL, Chen X, Burda C, Carlos WE (2005) Adv Funct Mater 15(1):161
29. Yamamoto Y, Moribe S, Ikoma T, Akiyama K, Zhang Q, Saito F, Tero-Kubota S (2006) Mol Phys 104(10–11):1733
30. Howe RF, Grätzel M (1987) J Phys Chem 91:3906
31. Qin H, Gu G, Liu S (2007) Rare Metals 26(3):254
32. Sakthivel S, Kisch H (2003) Chem Phys Chem 4:487